CHAPTER 7 RESULTS

7.1 The effect of the austenitisation temperature and holding time on the presence of undissolved particles in the V-Nb-Ti-containing alloys

Stable undissolved particles are important in the thermo-mechanically controlled process (TMCP) of line pipe steels. The finer austenite grain size after reheating and before entering the rough rolling stage, result in a good balance of strength and toughness of steels due to the existence of fine undissolved particles. These undissolved particles coarsen with increasing austenitisation temperature, which results in a coarse austenite grain size which is harmful to the final strength and toughness of the steel. The higher austenitisation temperature, however, is beneficial to the thermo-mechanical controlled process as it leads to a low deformation force in the rolling mill. Micro-alloying element additions to high-strength low carbon low alloy line pipe steels are necessary to, firstly, retard the growth of austenite grains at higher austenitisation temperatures and secondly, to retard deformation-induced recrystallisation in the final passes of hot rolling. In order to analyse these particles after reheating, two types of replicas were made in this work: carbon extraction replicas with and without Au-Pd shadowing.

The micrographs of the particles without shadowing are shown in figure 7.1 in which few and relatively small particles can be seen. This suggests that there is a low contrast between the small particles and the carbon film on the extraction replicas made without shadowing. In other words, this technique is not sensitive to small particles of less than 100 nm in diameter. For example, the small dark dot (shown by an arrow in figure 7.1-(b)) can not simply be identified as a particle. Some of the small particles, therefore, could not be included in the count for the calculation of the volume fraction of particles on normal unshadowed carbon replicas, which may have resulted in an error for the measured volume fraction of particles. In order to decrease this error, the technique of shadowed carbon extraction replicas was used to more clearly reveal the smaller particles. The carbon extraction replica with Au-Pd shadowing of alloy #6 after reheating at 1225 ºC for 120 min is illustrated in figure 7.2.

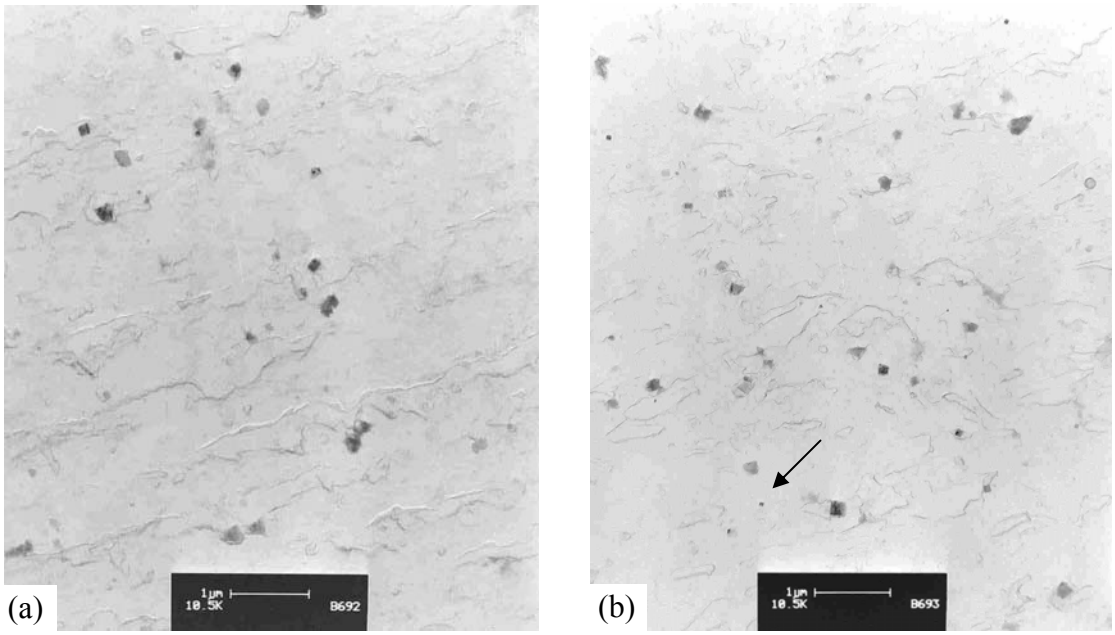

Figure 7.1 Extraction replicas without shadowing with undissolved particles for alloy #6 after reheating at 1200 ºC for 15 min. (Most of the darker spots are not particles but are etching debris on the replicas).

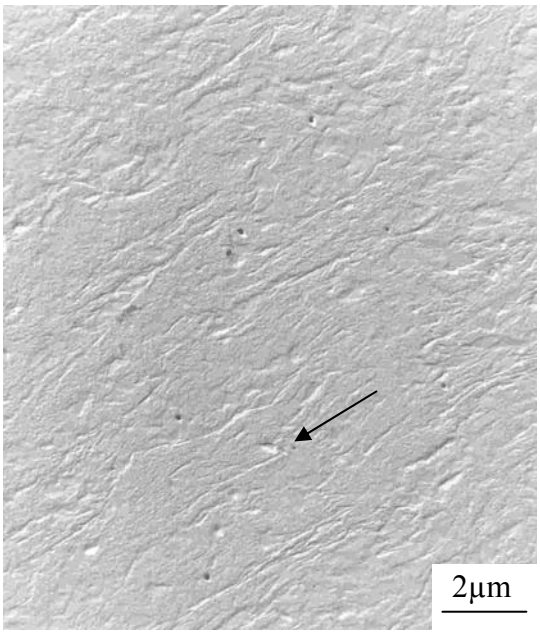

Figure 7.2 Extraction replicas with Au-Pd shadowing for alloy #6 after reheating at 1225 ºC for 120 min.

Comparing figures 7.1 (without shadowing) and 7.2 (with shadowing), the very small particles can be seen more clearly with shadowing, as shown by the small particle of about 52 nm in diameter (shown by an arrow in figure 7.2). It was easy to identify it as an undissolved particle and not etching debris as it contains a shadow beside it,

which indicates that the small particle was protruding from the surface during shadowing and before carbon evaporation. It was, therefore, concluded that the shadowed carbon extraction replica is superior in revealing undissolved particles than carbon extraction replicas without shadowing and this reduced errors in the measuring volume fraction of particles. Comparing the results of the volume fraction measurement of particles with and without shadowing, the measured volume fractions on shadowed replicas were higher than those without shadowing (see table 7.1 below). The volume fraction of particles was calculated in equations (6.1) and (6.2).

Table 7.1 Measured volume fraction of particles on replicas with/without shadowing in alloy #6

Treatment	**Volume fraction (%)**	
	No shadowing	**With shadowing**
As hot rolled	0.31	0.34
1200 ºC 15 min	0.26	0.27
1200 ºC 120 min	0.21	0.22

As may be seen in table 7.1, some smaller particles may not have been counted on unshadowed carbon replicas due to lack of adequate contrast with the carbon film. Therefore, the measured results on the shadowed replicas have a superior precision although both suffer from the effects of a lack of a planar surface after etching[127], which is a pre-requisite in the equation used to calculate the volume fractions.

Some TEM micrographs of particles on the shadowed replicas of alloy #6 after light etching in 2% Nital, are shown in figures 7.3, 7.4, 7.5 and 7.6 for the reheating treatments of 1150, 1200, 1225 and 1250 ºC for different times, respectively. Most undissolved particles are intragranular (marked with “A” in figure 7.6-(a)) and a few particles are on grain boundaries (marked with “B” in figure 7.6-(a)).

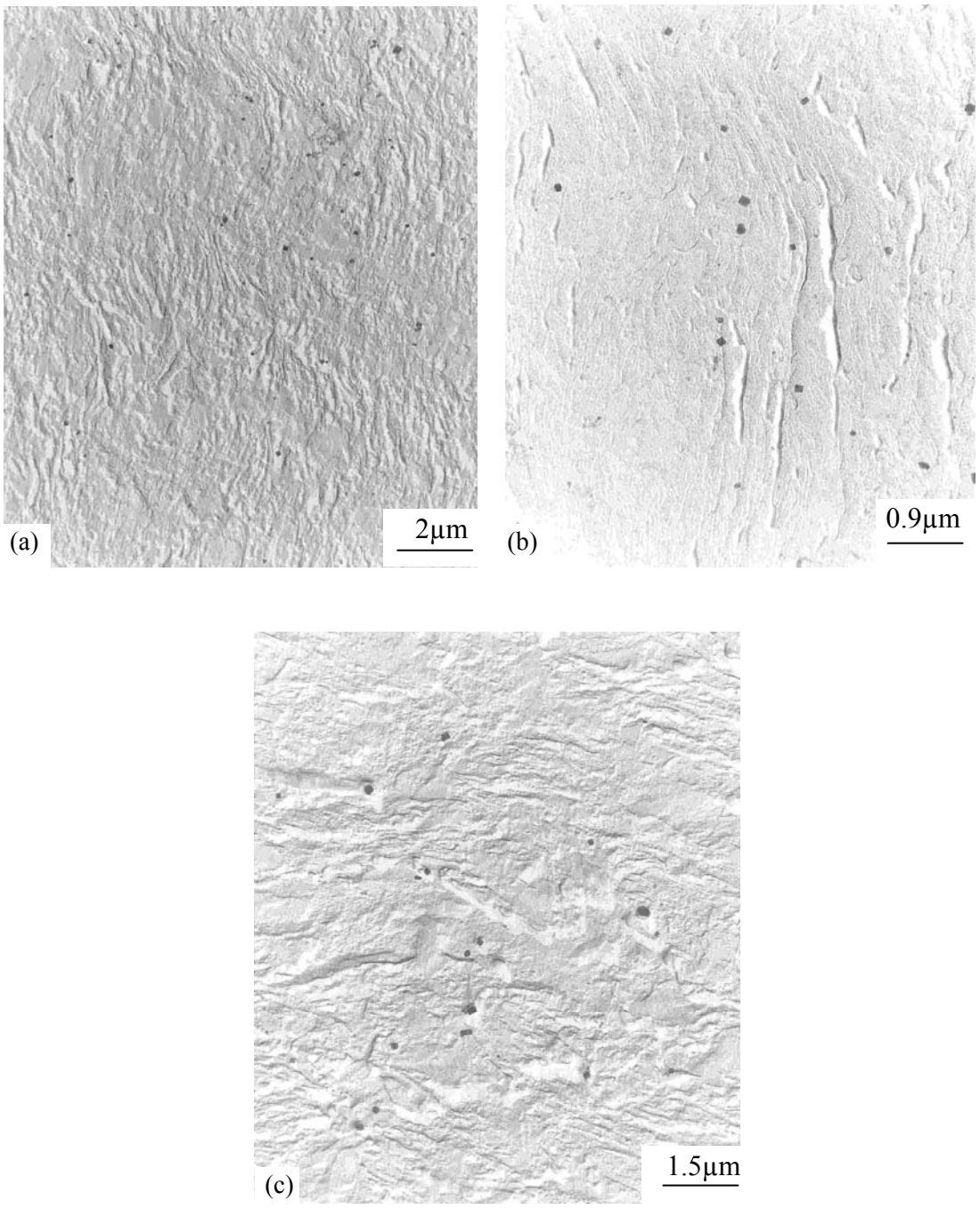

Figure 7.3 TEM micrograph of particles on the shadowed replicas of alloy #6 reheated at 1150 ºC for (a) 15 min, (b) 60 min and, (c) 120 min.

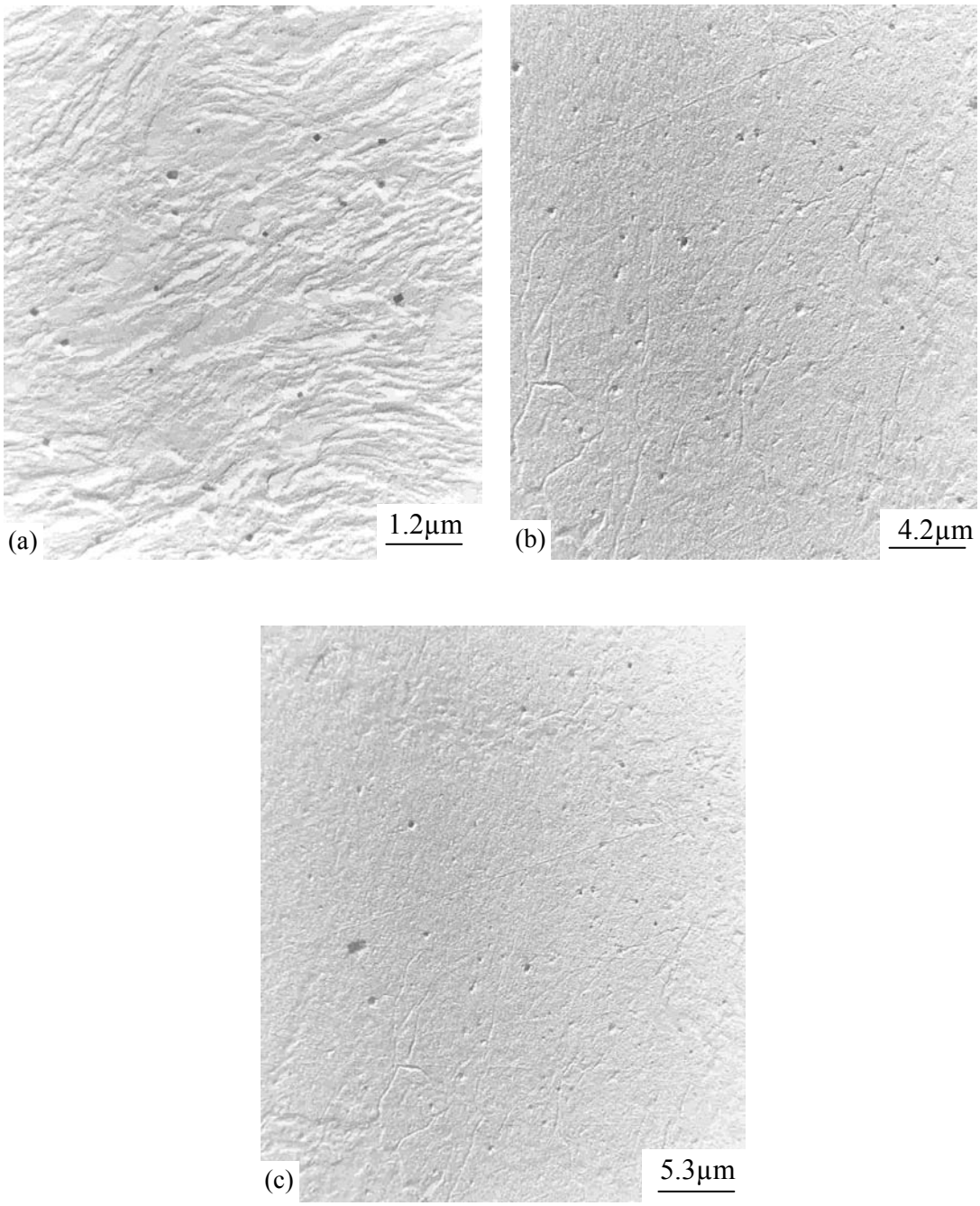

Figure 7.4 TEM micrograph of particles on the shadowed replicas of alloy #6 reheated at 1200 ºC for (a) 15 min, (b) 60 min and, (c) 120 min.

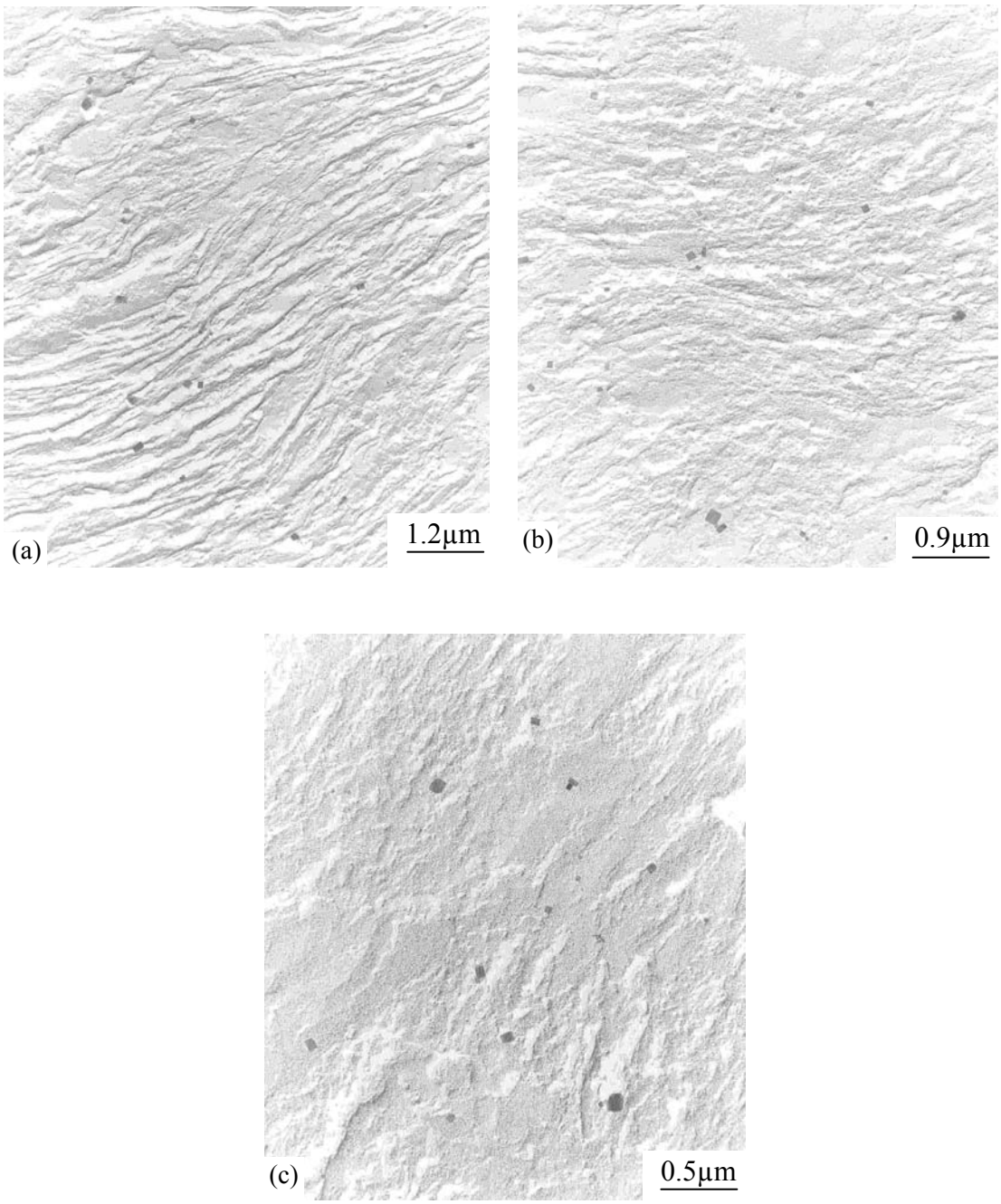

Figure 7.5 TEM micrograph of particles on the shadowed replicas of alloy #6 reheated at 1225 ºC for (a) 15 min, (b) 60 min and, (c) 120 min.

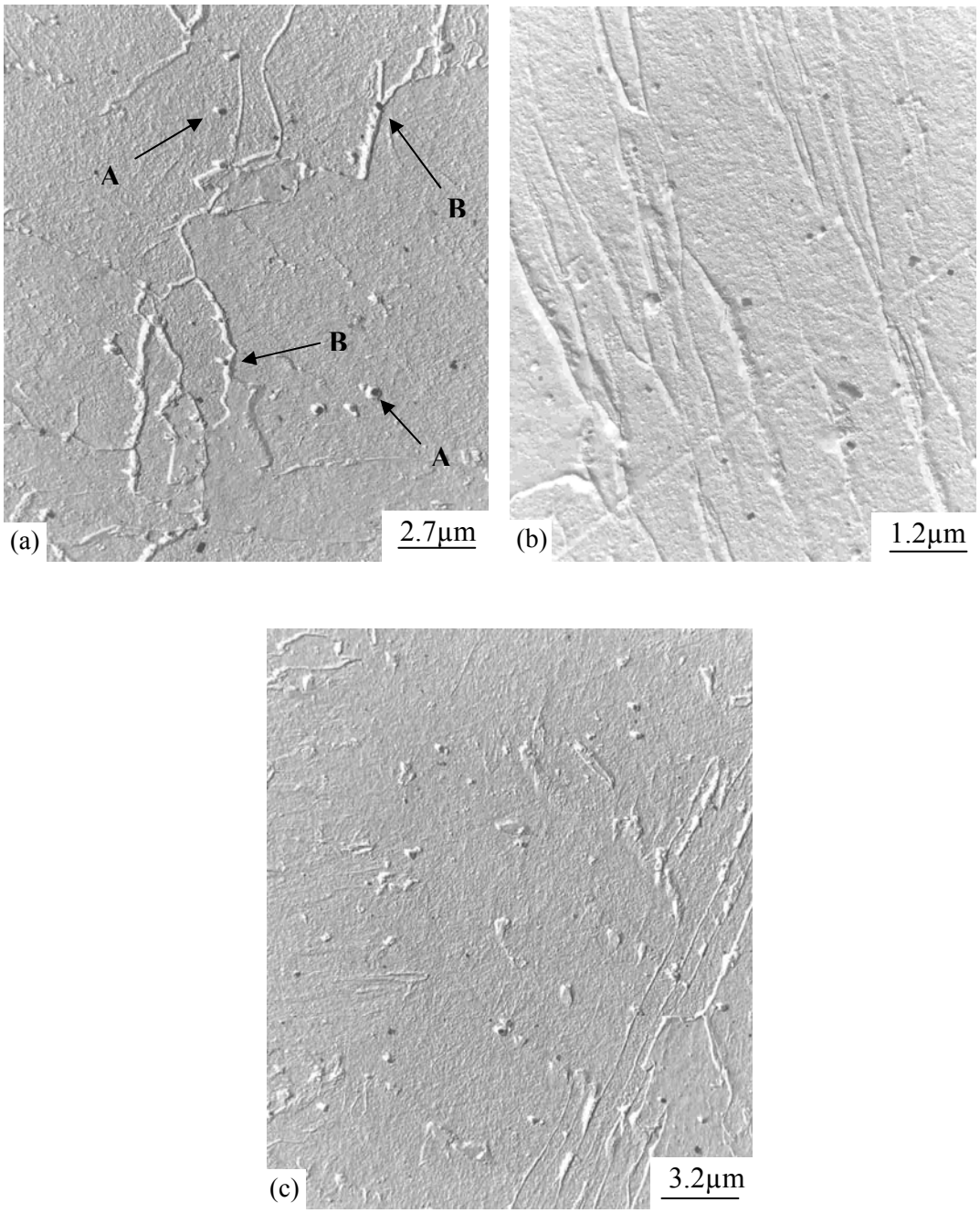

Figure 7.6 TEM micrograph of particles on the shadowed replicas of alloy #6 reheated at 1250 ºC for (a) 15 min, (b) 60 min and, (c) 120 min.

Table 7.2 is a summary of the measured results of undissolved particles observed on the shadowed replicas in the V-Nb-Ti micro-alloyed line pipe steel of Mittal Steel (alloy #6) whose chemical composition was given in table 6.1 in section 6.1.

Table 7.2 Undissolved particles: types and sizes after reheating treatments of alloy #6

Treatment		Type	Size in diameter (nm)	Shape	Nb/Ti Ratio of peak of EDS	Volume fraction (f_v,%)
As-hot rolled		(Ti,Nb)(C,N) (Ti,Nb)C (Nb,Ti)C VN	22~132 33~313 -- --	Square, Ellipsoid Square, Ellipsoid Square, Ellipsoid Square, Rectangle	0.31~0.39 0.22~0.8 4.11 --	*0.34*
1150 ºC	**15 min**	(Ti,Nb)N (Ti,Nb)(C,N)	132 24~94	Ellipsoid Square, Rectangle	0.13 0.21~0.28	0.32
	60 min	(Ti,Nb)(C,N) (Ti,Nb)C	25~132 56	Square Square, Rectangle	0.23~0.26 0.31	0.28
	120 min	(Ti,Nb)(C,N) (Ti,Nb)N (Nb,Ti)C	56~185 73~400 26	Square, Round Round, Square Round, Rectangle	0.21~0.43 0.21~0.27 10.7	0.26
1200 ºC	**15 min**	Ti(C,N) (Ti,Nb)N (Ti,Nb)(C,N)	46~132 182 27~313	Square Square, Rectangle Square	--- 0.18 0.15~0.29	*0.27*
	60 min	(Ti,Nb)(C,N) (Ti,Nb)N	29~330	Square, Rectangle		0.24
	120 min	(Ti,Nb)(C,N) (Ti,Nb)N	22~182 94 ~382	Square, Rectangle Square, Rectangle	0.12~0.16 0.11~0.21	*0.22*
1225 ºC	**15 min**	(Ti,Nb)(C,N) Ti(C,N)	27~322	Square, Rectangle	--	0.22
	60 min	(Ti,Nb)(C,N) Ti(C,N)	25~396	Square, Rectangle	--	0.21
	120 min	(Ti,Nb)(C,N)	30~375	Square, Rectangle	--	0.19
1250 ºC	**15 min**	(Ti,Nb)(C,N) Ti(C,N)	37~428	Square, Rectangle	--	0.21
	60 min	(Ti,Nb)(C,N)	34~403	Square, Rectangle	--	0.20
	120 min	(Ti,Nb)(C,N) Ti(C,N)	46~439	Square, Rectangle	--	0.19

As can be seen from table 7.2, the types of undissolved particles are (Ti,Nb)(C,N), (Ti,Nb)C, (Ti,Nb)N, Ti(C,N) and (Nb,Ti)C. Their respective shapes are cubic or squared, rectangular, rounded and ellipsoidal. There were some VN particles in the as-hot rolled condition but no VN particles were observed after reheating treatments

above 1150 ºC in alloy #6. VN particles were completely dissolved in the austenite above 1150 ºC in this steel and, therefore, can not inhibit the grain growth of the austenite above this temperature.

(Ti,Nb)C and (Nb,Ti)C particles of ellipsoidal and rounded shapes appeared to dissolve at 1200 ºC after 120 min. (Ti,Nb)(C,N) and (Ti,Nb)N remained undissolved at this temperature as indicated by the fact that only square and rectangular particles remained in the steel. It was observed that these squared and rectangular particles were more stable than the ellipsoidal and rounded ones with increasing solution temperature. Some EDS spectra from the transmission electron microscope analyses are presented in figure 7.7.

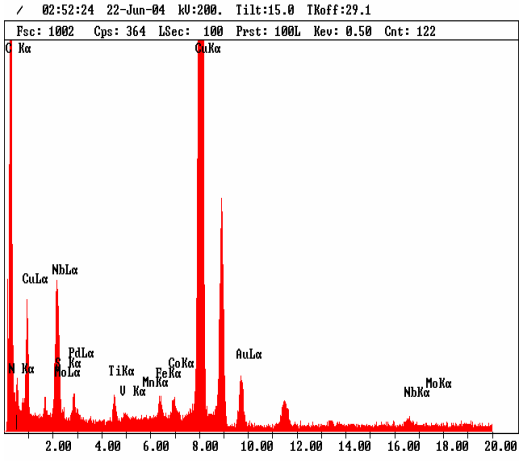

(a) (Nb,Ti)C

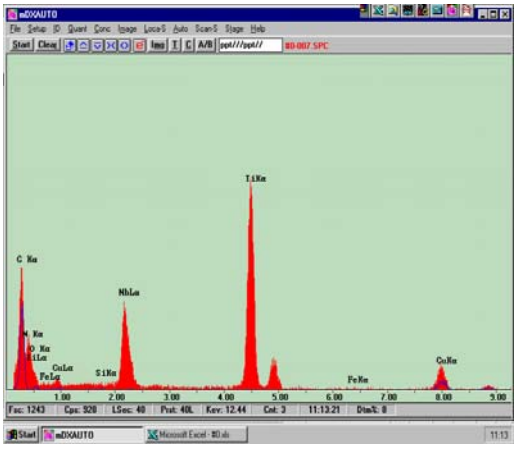

(b) (Ti,Nb) (C,N)

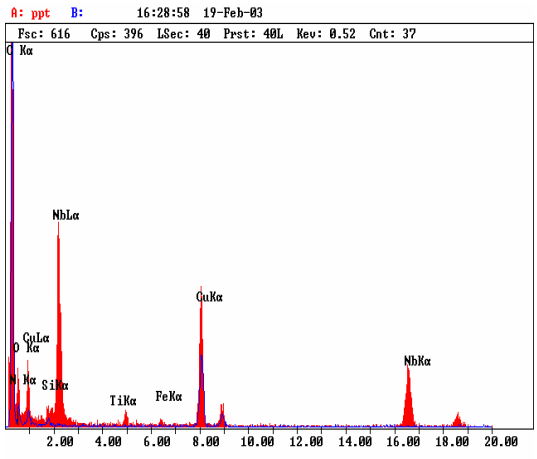

(c) (Nb,Ti) C

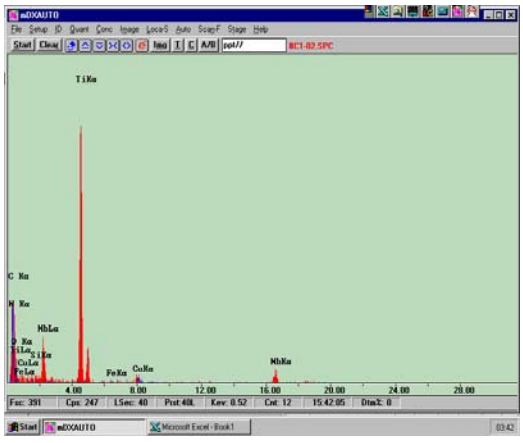

(d) (Ti,Nb)N

Figure 7.7 TEM-EDS results of undissolved particles of alloy #6 after the treatments of (a) as-hot rolled, (b) as-hot rolled, (c) 1150 ºC for 120 min and, (d) 1200 ºC for 15 min.

Some copper peaks in figure 7.7 were probably from the copper grid that supports the carbon coating while a large part of the carbon from the carbon peak (marked with blue) was from the background of the carbon replicas films.

As may be expected in figure 7.8, the volume fractions (f_v) of undissolved particles decreases with an increase in the temperature of solution treatment for all the investigated soaking times, i.e. 15, 60 and 120 min. The curve fitted equations are as follows for the times of 15, 60 and 120 min, respectively.

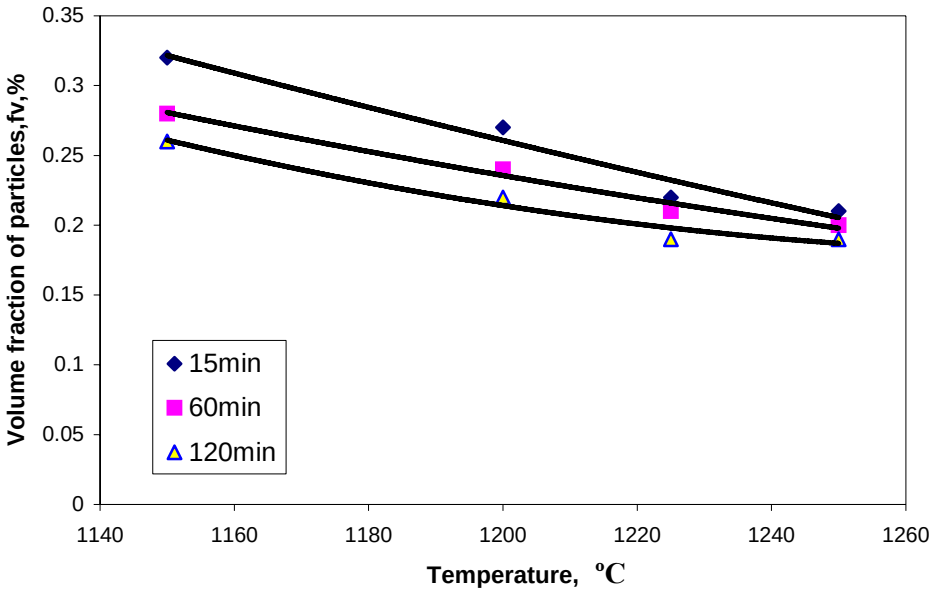

Figure 7.8 The effect of reheating temperature and time on the volume fraction of undissolved particles for alloy #6.

$f_v=10^{-6}T^2-0.0038T+3.2258$ $R^2=0.97$ for 15min soaking time (7.1)

$f_v=10^{-6}T^2-0.0043T+3.3251$ $R^2=0.99$ for 60min soaking time (7.2)

$f_v=4\times10^{-6}T^2-0.0103T+6.862$ $R^2=0.97$ for 120min soaking time (7.3)

where f_v is volume fraction of undissolved particles after the soaking time in %.

T is temperatures of solution or reheating treatment in ºC.

R^2 is the regression fitting coefficient.

As can be seen from equations (7.1) to (7.3), there is a similar trend between the volume fraction of undissolved particles and the solution or reheating temperature at different soaking times. The undissolved particles become less stable at higher

solution temperatures and, therefore, reduce their ability to inhibit any growth of the austenite grains. It can, therefore, be concluded that at high solution temperatures, small particles dissolve and large ones coarsen and the grain boundary pinning effect is reduced or eliminated, leading to austenite grain growth.

There are two effects in the present work: one is coarsening at constant temperature by small particles dissolving and large particles growing by the Lifshitz-Slyosov-Wagner process, such as with the more stable (Ti,Nb)(C,N) and Ti(C,N) that will coarsen above 1250 ºC for 120 min (see table 7.2). The second effect arises from a larger solubility at higher temperatures in which all sizes of particles dissolve, i.e. both small and large ones dissolve, such as with the less stable VN at 1150 ºC and (Ti,Nb)C, (Nb,TI)C at 1200 ºC. This latter type of particle is less stable than the former ones, so that they lose any effect to inhibit the growth of austenite grains.

Table 7.2 shows that the size of the smallest undissolved particles does not significantly change below 1225 ºC. The smallest sizes for the as-received as-hot rolled steel of alloy #6 was 22 nm and after soaking at 1225 ºC for 120 min, this size increased to about 30 nm. The particles started coarsening at a soaking temperature of 1250 ºC for 120 min when a mean particle diameter of 46 nm was observed. It can be concluded that the undissolved particles in alloy #6 containing Nb-Ti-V micro-alloying elements, still had a strong inhibition on the growth of the austenite grains and, therefore, fine austenite grains can still be obtained at reheating temperatures up to about 1225 ºC. The particles of Ti- or (Ti+Nb)-carbonitrides, however, were still undissolved at temperatures above 1200 ºC. All of the V- and Nb-carbides and V-nitrides were dissolved completely at temperatures above 1200 ºC, meaning that only Ti- and (Ti+Nb)-carbonitrides or nitrides contribute to a grain boundary pinning effect to limit austenite grain growth above the temperature of 1200 ºC. In order to get much greater dispersion hardening (Nb- and V-carbides in ferrite) and stronger retarding of austenite grain growth (undissolved particles of Ti- or (Ti+Nb)-carbonitrides in austenite), enough titanium in the steel is needed to bind all free nitrogen, leading to a significant increase in niobium available in the ferrite. In conclusion: if the reheating temperature in the hot rolling process is not more than 1225 ºC, a combination of

greater dispersion hardening and smaller austenite grains after reheating may still be achieved in Nb-Ti micro-alloyed steels.

7.2 Austenite grain size and reheating temperature

The reheating temperature should be high enough to dissolve most of the micro-alloying elements without significant growth of the austenite grains, but also allowing dispersion hardening after the TMCP. The in-situ carburising technique by carbon monoxide gas was used to reveal austenite grain boundaries. The austenite grain size for alloy #6 is shown in figures 7.9 (a)-(d) for reheating conditions at 1150 to 1250 ºC, respectively.

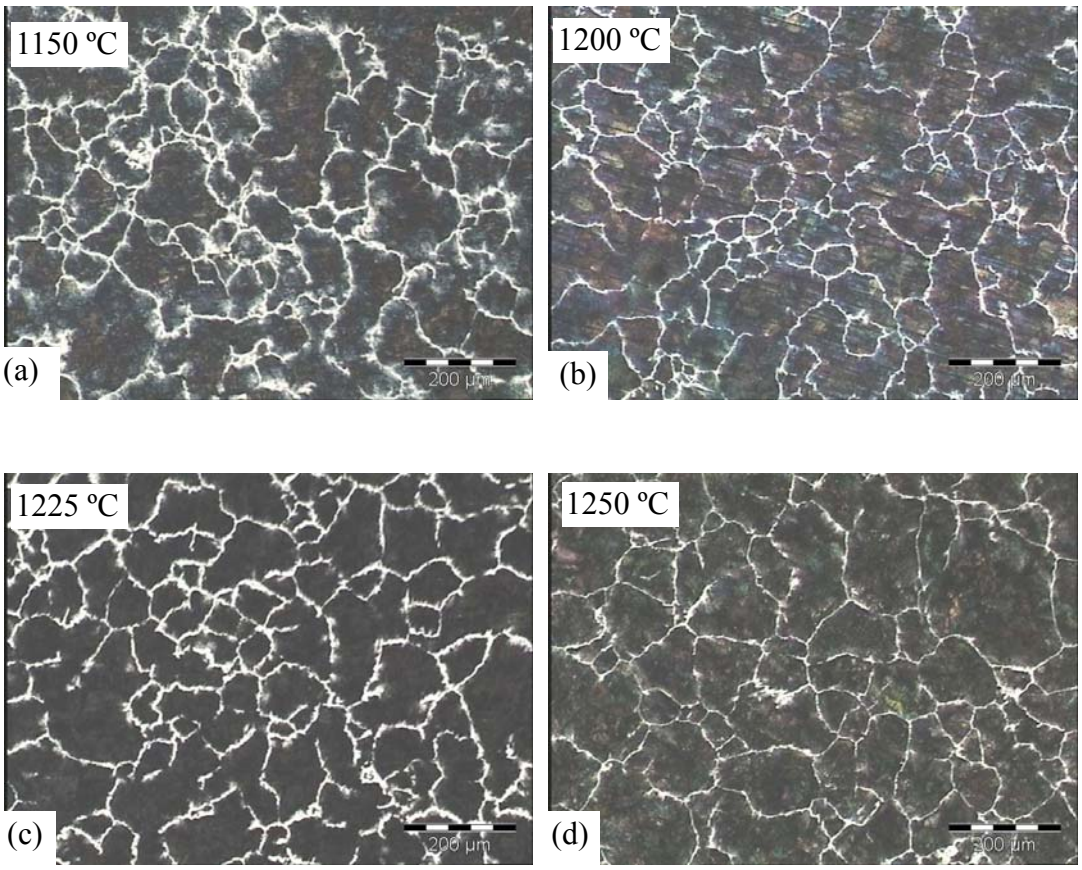

Figure. 7.9 Pro-eutectoid cementite decorates the original austenite grain boundaries in alloy #6 for soaking times of 60 min at different austenitisation temperatures.

The measured intercept length of the austenite grain size for each treatment is shown in table 7.3 below as well as in figures 7.10 and 7.11 while some data from the literature[39] for a steel with composition of 0.1% C, 0.2% Si, 1.4% Mn, 0.005%N, 0.03% Al and 0.01% Ti, have been included in figure 7.10 as a reference.

Table 7.3 Intercept length austenite grain size, in µm, versus reheating temperature and soaking time of alloy #6

Soaking time	1150 ºC	1200 ºC	1225 ºC	1250 ºC
15 min	32.3	41.6	50.4	65.5
30 min	33.9	49.6	52.9	75.0
60 min	48.9	53.0	57.1	76.5
120 min	54.0	58.7	62.9	82.7

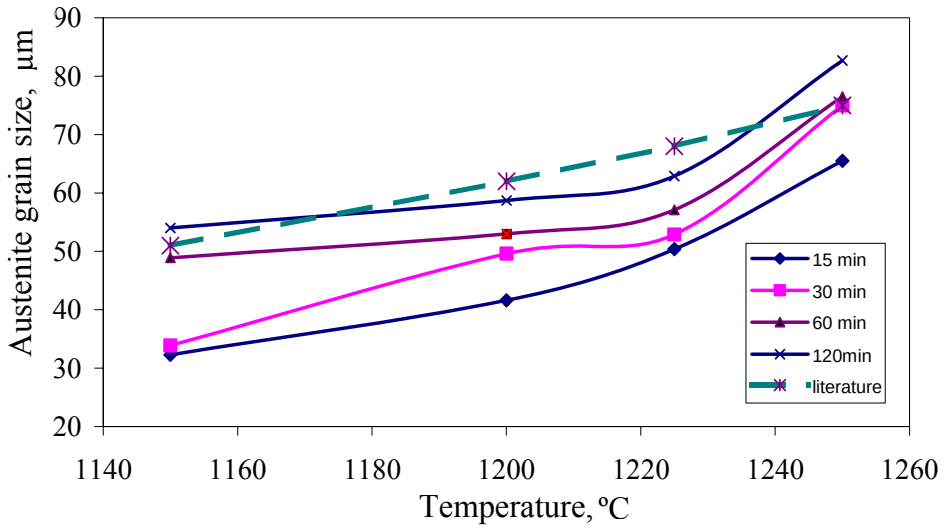

Figure. 7.10 The relationship between the austenitisation temperature and the austenite grain size for alloy #6. The broken line is from published data[39].

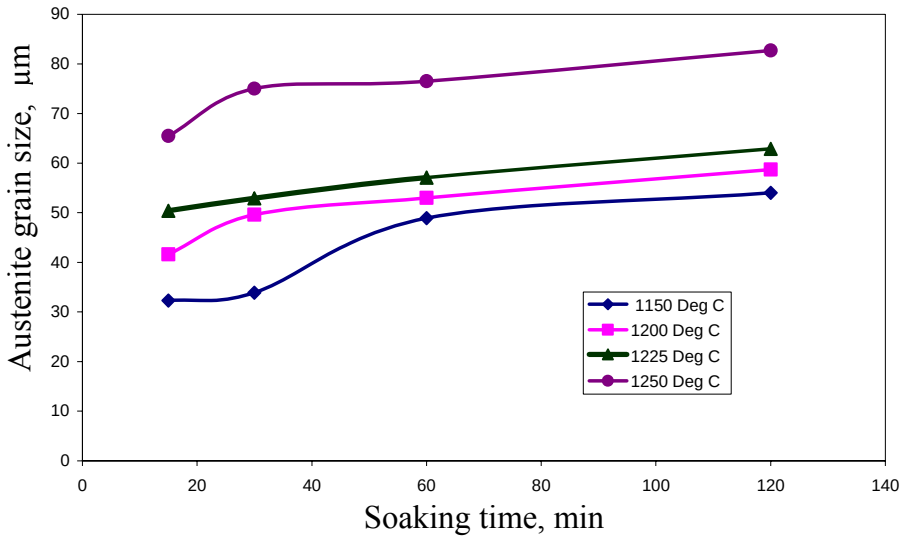

Figure. 7.11 The weak effect of soaking time on the austenite grain size for alloy #6.

As may be seen from figure 7.10, the austenite grain size for alloy #6 increased with increasing austenitisation temperature from 1150 to 1250 ºC, at a constant soaking time. The austenite grains grow slowly, however, below 1225 ºC due to the pinning of the grain boundaries by the stable micro-particles, i.e. (Ti,Nb)(C,N) or (Ti,Nb)N as described in section 7.1, as there is less coarsening of these carbonitrides in the alloy below 1225 ºC. Significant coarsening begins, however, when the carbonitrides dissolve at 1250 ºC (see figure 7.10). As a result, the austenite grains grow sharply with an increase in temperature above 1225 ºC. The growth in austenite grain size is given by an increase of ΔD=19.8 µm from 1225 to 1250 ºC for a soaking time of 120 minutes, compared to a growth by an increase of only ΔD=4.2 µm from 1200 to 1225 ºC. Accordingly, the reheating temperature of the alloys in the present study should not be higher than 1225 ºC for a relatively fine austenite grain size.

Considering much greater dispersion hardening in the ferrite from Nb-bearing precipitates and raising the non-recrystallisation temperature, the niobium should preferably be dissolved completely into the matrix of the steel. The reheating temperature before the hot rolling process should, therefore, not be too low also, but so high that all of the niobium could dissolve into the matrix of the steel. The most effective precipitation strengthening, therefore, can be obtained from NbC precipitation in ferrite[12]. A higher non-recrystallisation temperature (T_{nr}) can also be obtained[12] due to the precipitation of Nb(C,N) during hot rolling[28]. This will, on the

other hand, result in "pancake" austenite grains during hot rolling, providing more nucleation sites as well as sufficient strain accumulation for the following ferrite formation, which results in finer ferrite. Cuddy[114] reported that the broad range of initial austenite grain sizes (53 to 325 μm) converged to a narrow range of grain sizes of 43 to 53 μm after multiple recrystallisation that was produced by a five passes reduction schedule. It was also found that the final austenite grain size before reaching the T_{nr} was dependent mainly on the deformation parameters and was largely independent of the steel's composition, i.e. similar for C-Mn, Nb-bearing and V-bearing steels. Considering a combination of finer austenite grains and greater dispersion hardening, the limit of 1225 ºC was taken as the most appropriate reheating temperature in this study. On the other hand, niobium also raises the T_{nr} because of solute drag by niobium on austenite boundaries if niobium is completely dissolved into the steels. A higher Nb addition, therefore, results in more deformation below the T_{nr} during the hot rolling (if compared to that of lower Nb additions) which induces a finer ferrite grain size.

The soaking time at the austenitisation temperature influences the austenite grain size as well although to a lesser extent than the temperature. The longer the soaking time, the larger the austenite grain size (see figure 7.11). The soaking time is, therefore, largely determined by the slab's section size to achieve uniform temperatures and also to a lesser extent, by the need to dissolve the niobium micro-alloying elements.

7.3 The non-recrystallisation temperature (T_{nr}) and deformation parameters

The non-recrystallisation temperature (T_{nr}) is one of the most important factors in the design of the thermo-mechanically controlled process (TMCP) schedule for line pipe steels. The T_{nr} is the critical temperature below which no dynamic or static recrystallisation will take place during or immediately after hot rolling and this leads to the formation of so-called "pancake" grains. The austenite grains become flattened with consecutive pass reductions as the strain accumulates, up to the Finishing Mill Head where after transformation to ferrite takes place on the run-out table. The finishing rolling is normally carried out below the T_{nr}, which is a function of the alloy content (particularly the Nb alloying addition) as well as parameters of the TMCP, i.e. pass strain (ε), strain rate($\dot{\varepsilon}$) and inter-pass time (t_{ip}).

7.3.1 The T_{nr} and pass strain

Figure 7.12 illustrates for alloy #6 the compression deformation cycles used at various pass strains ranging from 0.15 to 0.32 at the same strain rate of 1 s^{-1} and inter-pass times of 8 seconds.

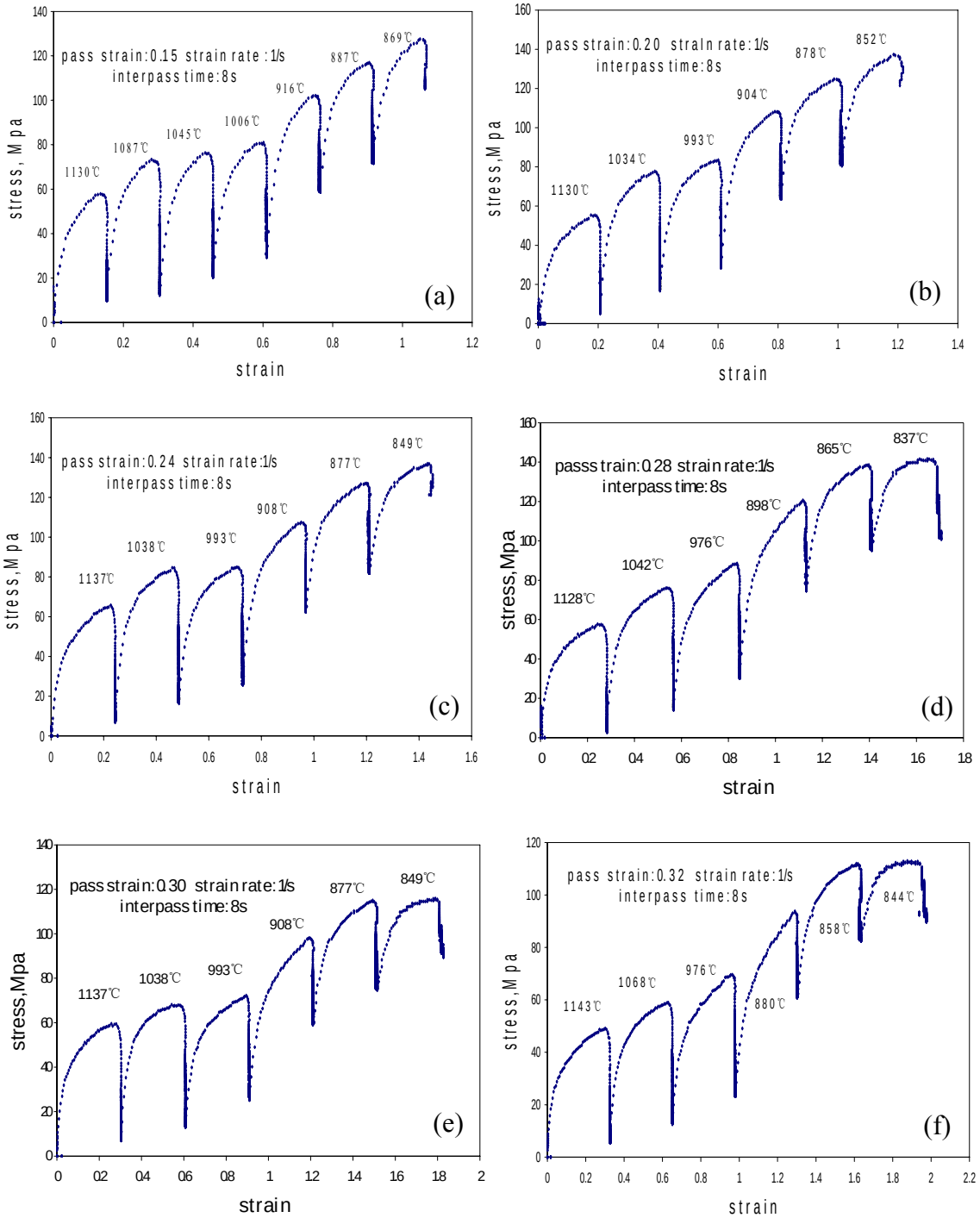

Figure 7.12 Stress-strain curves of multi-pass compression tests of alloy #6 at the same strain rate of 1 s^{-1}, inter-pass time of 8 seconds and different pass strains.

The number of passes in these compression tests was seven at 0.15 strain per pass and 6 passes at more than 0.2 strain per pass. The stress-strain curves for each pass are presented in figure 7.12 with the temperatures of each pass marked on its stress-strain curve. The mean flow stress of each pass was then calculated according to equation (6.4) and the curves of the mean flow stress with the inverse pass deformation temperature plotted as shown in the following figure 7.13. Two straight lines can be obtained here: one has a lower slope at the higher temperature range and the other has a higher slope at the lower temperature range. When the deformation takes place below the T_{nr}, the slope in figure 7.13 increases because of the retained strain hardening within the non-recrystallisation region. As may be seen in figure 7.13, a point of intersection is obtained, which is the non-recrystallisation temperature marked by an arrow (T_{nr}).

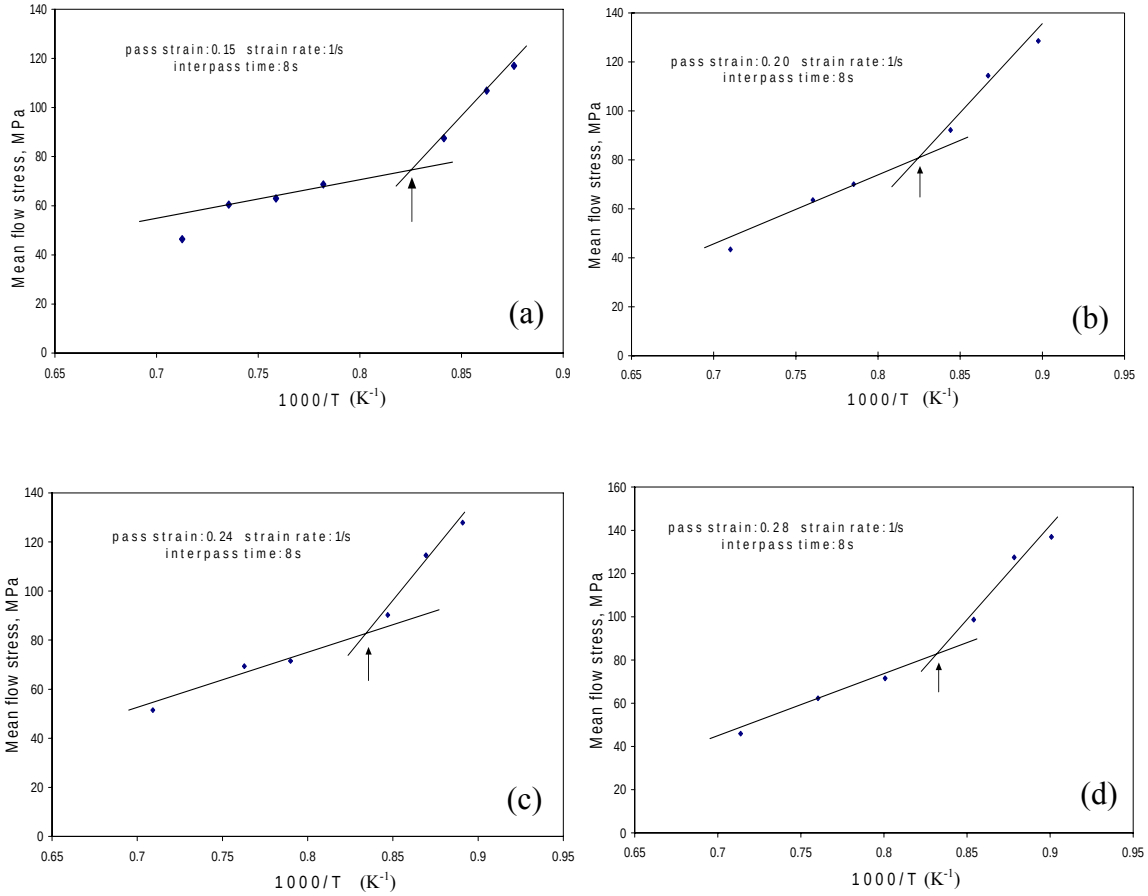

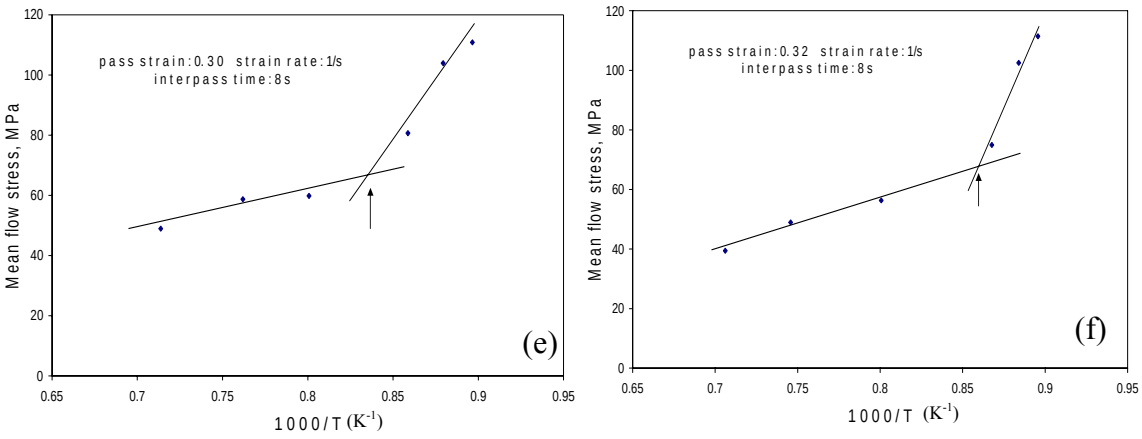

Figure 7.13 Determination of the T_{nr} on the mean flow stress versus inverse temperature curves of alloy #6, all deformed at the same strain rate of 1 s^{-1} and an inter-pass time of 8 seconds but at different pass strains.

As may be seen in figure 7.13, the slope of the straight line below the T_{nr} is lower at a low pass strain of 0.15 than at a strain of 0.32 per pass. The slope of the straight line below the T_{nr}, therefore, appears to increase with an increase in pass strain. This is because the accumulation of retained strain from pass to pass during non-recrystallisation, is higher at higher pass strains. The higher pass strain induces a higher density of dislocations in the flattened austenite grains, which will remain below the T_{nr}, until transformation to ferrite occurs on the run-out table. The results of the T_{nr} at various pass strains are listed in table 7.4 for alloy #6 and are also shown in figure 7.14.

Table 7.4 The non-recrystallisation temperature and pass strains of alloy #6

Sample number	**A15**	**A20**	**A24**	**A28**	**A30**	**A32**
Inter-pass time, t_{ip} (s)	8	8	8	8	8	8
Strain rate (s^{-1})	1	1	1	1	1	1
Pass strain ε	0.15	0.2	0.24	0.28	0.30	0.32
T_{nr} (°C)	937	931	922	916	918	893

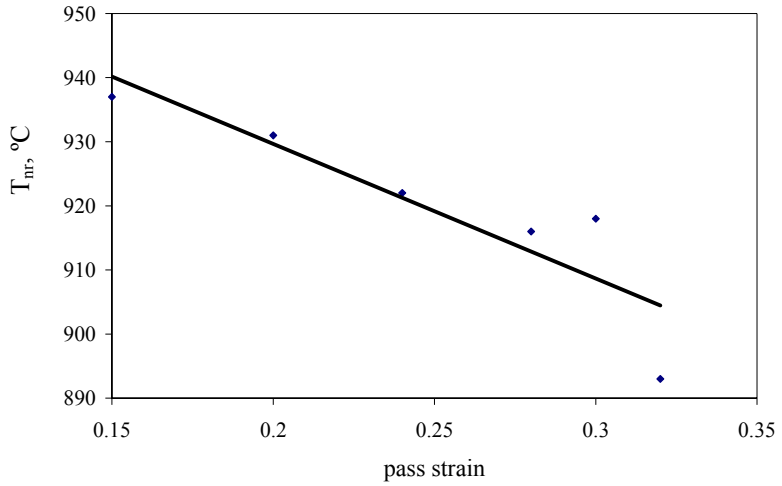

Figure 7.14 The relationship between pass strain (ε) and the non-recrystallisation temperature for alloy #6. Strain rate $\dot{\varepsilon}$ =1.0 s^{-1}, inter-pass time t_{ip}=8 s.

The strain rate and inter-pass time were held constant at $\dot{\varepsilon}$ =1.0 s^{-1} and t_{ip}=8 s in this series of tests. The T_{nr} in the Mo-free reference alloy #6 decreases with increasing pass strain in an approximately linear relationship. The tendency of the T_{nr} versus pass strain is consistent with the results of Cuddy et al[128] and Bai et al[48,125], i.e., the T_{nr} decreases with an increase in pass strain. This quantitative relationship in alloy #6 can be described by the following equation:

$$T_{nr} = -210\,\varepsilon + 972 \qquad R^2 = 0.79 \qquad (7.4)$$

where T_{nr} is in ºC and the strain ε expressed as the true strain.

Above the T_{nr} grain refinement significantly increases the dislocation density during hot working and this encourages the coarsening of precipitates[111]. As the pass strain increases, austenite grains become finer. The higher dislocation density is associated with a higher stored energy in the austenite, which constitutes the driving force for recrystallisation. Therefore, increasing the pass strain promotes austenite recrystallisation and lowers the T_{nr}. Furthermore, the coarser particles have little effect on retarding the austenite recrystallisation[125]. Weiss and Jonas[112], Bai et al[125] and Speer and Hansen[113] reported that precipitate coarsening during hot deformation takes place as the pass strain increases and these larger particles lose their ability to retard recrystallisation.

7.3.2 The T_{nr} and inter-pass time

The inter-pass time also affects the non-recrystallisation temperature during the hot rolling process. The hot compression results at various inter-pass times ranging from 4 to 50 seconds, with the same pass strain of 0.2 and strain rate of 1 s^{-1} for alloy #6, are shown in figure 7.15.

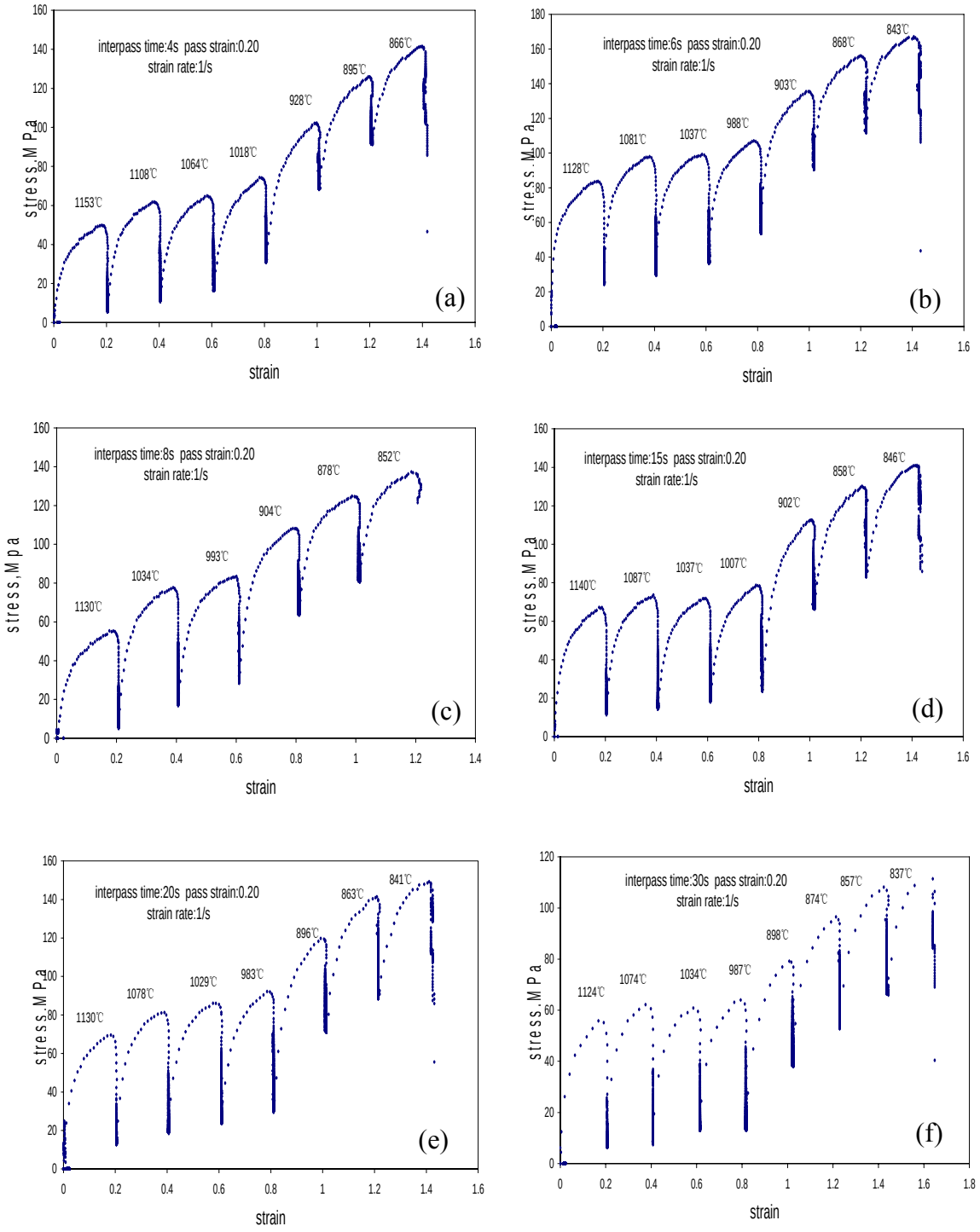

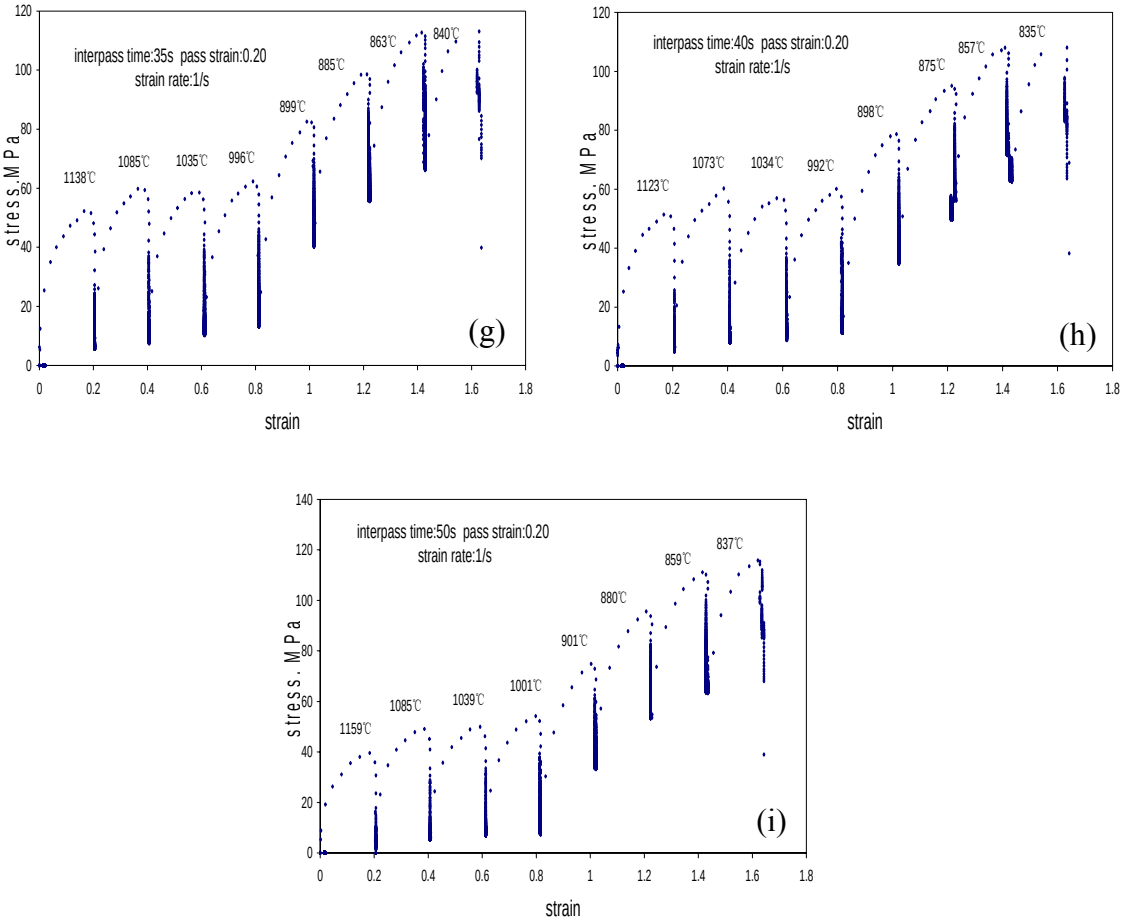

Figure 7.15 Stress-strain curves of multi-pass compression tests on alloy #6 at a constant pass strain of 0.20, a constant strain rate of 1 s^{-1} and a series of inter-pass times ranging from 4 to 50 seconds.

The number of passes in these tests is 6, 7 or 8 (some results were obtained on the Gleeble before its upgrading, others after the upgrading. From there a difference in number of passes arose). The pass temperature is also marked on the respective figures. The mean flow stress values calculated from figure 7.15 is plotted against the inverse pass temperature (in K) in figure 7.16.

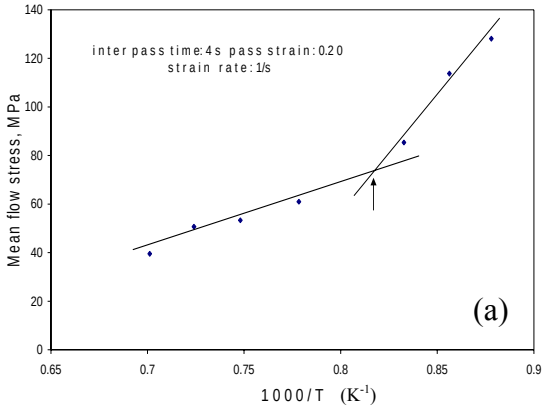
inter pass time:4s pass strain:0.20
strain rate:1/s
Mean flow stress, MPa
1000/T (K-1)
(a)

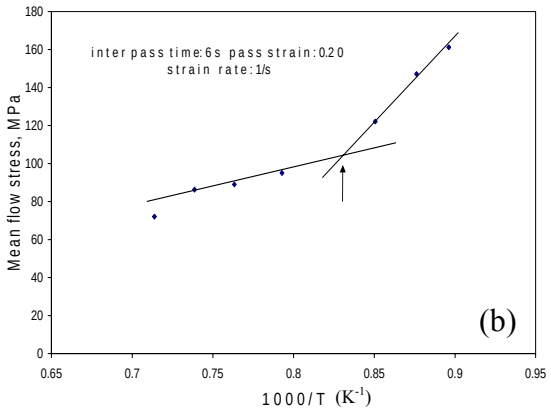
inter pass time:6s pass strain:0.20
strain rate:1/s
Mean flow stress, MPa
1000/T (K-1)
(b)

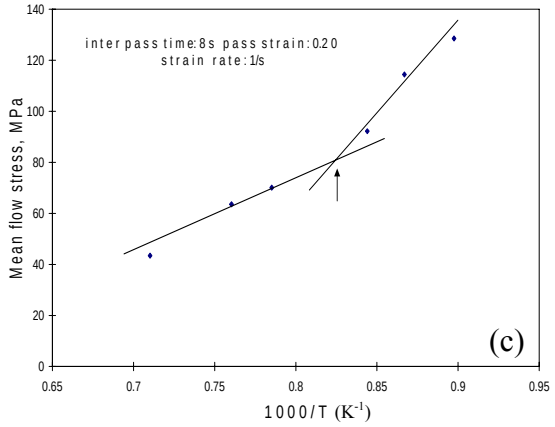
inter pass time:8s pass strain:0.20
strain rate:1/s
Mean flow stress, MPa
1000/T (K-1)
(c)

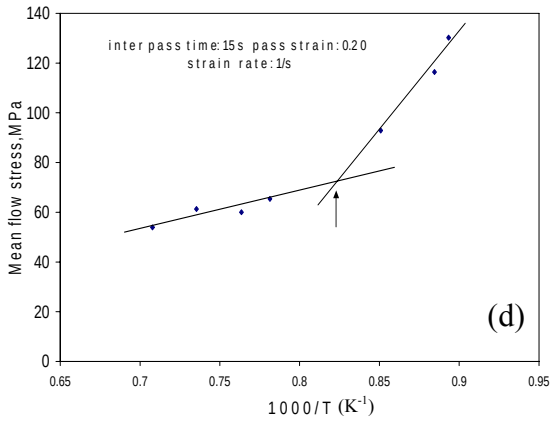
inter pass time:15s pass strain:0.20
strain rate:1/s
Mean flow stress,MPa
1000/T (K-1)
(d)

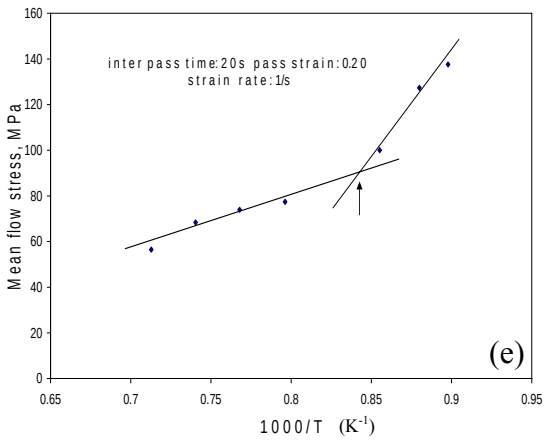
inter pass time:20s pass strain:0.20
strain rate:1/s
Mean flow stress, MPa
1000/T (K-1)
(e)

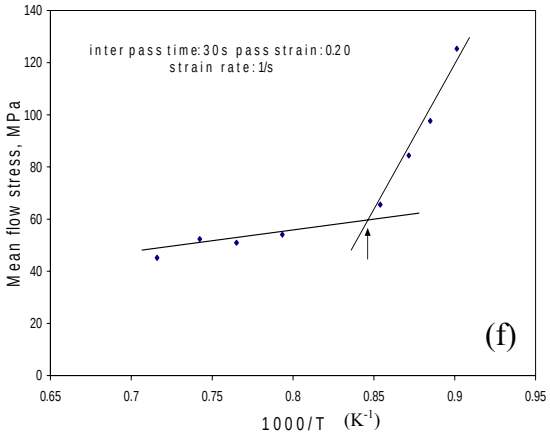
inter pass time:30s pass strain:0.20
strain rate:1/s
Mean flow stress, MPa
1000/T (K-1)
(f)

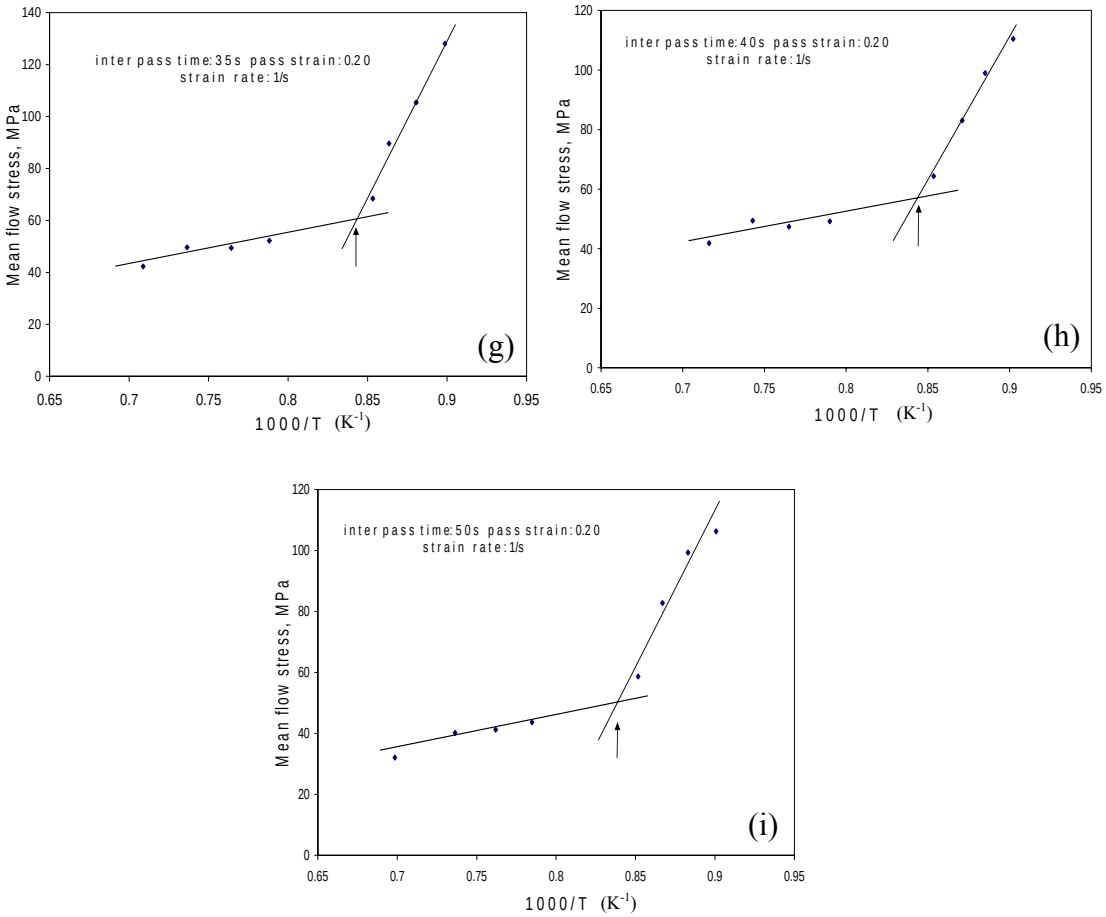

Figure 7.16 The mean flow stress versus inverse temperature curve of alloy #6 during multi-pass compression testing at a constant pass strain of 0.20 and a constant strain rate of 1 s^{-1} but with a variation of the inter-pass times between 4 and 50 seconds.

The values for T_{nr} obtained from figure 7.16 at various inter-pass times are summarised in table 7.5 and figure 7.17.

Table 7.5 The non-recrystallisation temperature of alloy #6 as affected by different inter-pass times

Sample number	**D4a/4b**	**D6**	**D8**	**D15a/15b**	**D20**	**D30**	**D35**	**D40**	**D50**
Pass strain, ε	0.2	0.2	0.2	0.2	0.2	0.2	0.2	0.2	0.2
Strain rate (s^{-1})	1	1	1	1	1	1	1	1	1
Inter-pass time, t_{ip} (s)	4	6	8	15	20	30	35	40	50
T_{nr} (ºC)	934/ 956	938	931	941/ 921	930	914	916	921	913

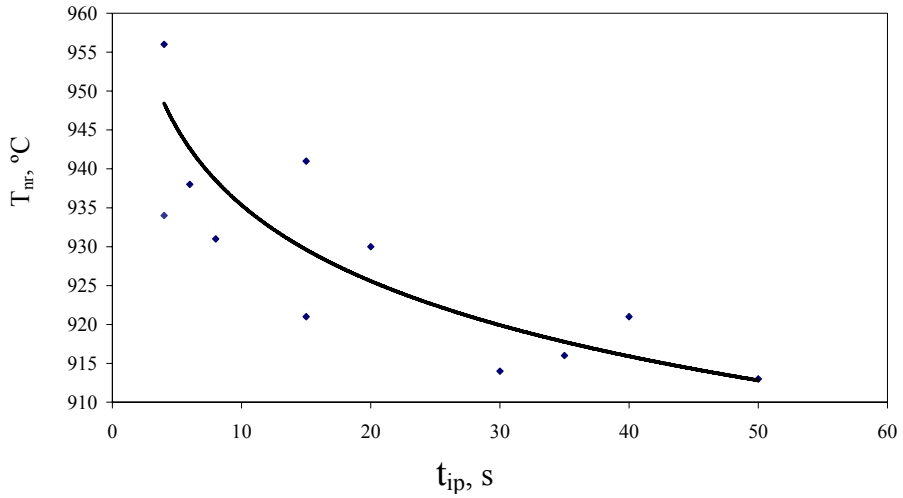

Figure 7.17 The T_{nr} as a function of inter-pass time (t_{ip}) for alloy #6. Strain rate $\dot{\varepsilon}$ =1.0 s^{-1}, pass strain ε = 0.2.

It can be seen that the T_{nr} decreases with increasing inter-pass time from 4 to 50 seconds in alloy #6. Although a large degree of scatter was present, this dependence can be described approximately by the following equation:

$$T_{nr}=961t_{ip}^{-0.0128} \qquad R^2=0.68 \qquad (7.5)$$

The result is different from that of Bai[48,125]. Bai reported that the dependence of the T_{nr} can be divided into three distinct regions: short inter-pass times (less than 12.5 seconds), medium inter-pass times (from 12.5 to 80 seconds) and long inter-pass times (more than 80 seconds). Within the short inter-pass times, the T_{nr} decreases with an increase in inter-pass time up to 12.5 seconds because solute drag by Nb on austenite grain boundaries retards recrystallisation prior to precipitation of NbC. Within the medium inter-pass times, precipitation of NbC occurs and retards recrystallisation and the T_{nr} then increases with an increase in inter-pass time. With a further increase in inter-pass time, the precipitates become coarse and become less effective in retarding the recrystallisation, so that the T_{nr} decreases again with inter-pass time. Some researchers[17,27,129] supported this finding of Bai while another[106] supported the key mechanism of a process of strain induced precipitation.

In this study, it was found that the T_{nr} decreases with increasing inter-pass time within the range of 4 to 50 seconds, probably with both solute drag and precipitation that

affect the recrystallisation. The dependence of the T_{nr} on inter-pass time can be divided into two regions: short inter-pass times (t_{ip}<20 s) and long inter-pass time (20<t_{ip}<50 s). In the short inter-pass times, deformation induces a high density of dislocations and point defects[130] that are beneficial to the nucleation of austenite recrystallisation. Solute drag by Nb on austenite grain boundaries prior to precipitation plays only a retarding role in recrystallisation, which probably is weaker in this range, while dislocations and point defects provide enough driving force for recrystallisation. This means that more recrystallisation will takes place with increasing inter-pass time, leading to a sharp decrease in the T_{nr} with an increase in inter-pass time. With a further increase in inter-pass time, i.e. more than 20 seconds, the effect of inter-pass times on the T_{nr} becomes less. Precipitation takes place and the precipitates are still fine (coarsening is only significant after 80 seconds[125]) in this stage as there is enough time for Nb(C,N) or NbN nucleation on the dislocations introduced from the deformation[130]. These finer precipitates pin the grain boundaries, so that the retarding effectiveness of Nb(C,N) or NbN particles on the recrystallisation is significant. This means that the effect of inter-pass time could become weaker at longer times. Figure 7.17 showed that the effect of the precipitation on the recrystallisation is, therefore, probably stronger than that of solute drag. However, the effect of the precipitates of Nb(C,N) or NbN appears to be not greater than that found by Bai[125].

7.3.3 The T_{nr} and pass strain rate

The T_{nr} can also be affected, besides by the pass strain and inter-pass time, also by the pass strain rate during compression deformation. A group of tests at a pass strain rate ranging from 0.1 to 2.22 s^{-1} was carried out at a constant pass strain of 0.20 and a constant inter-pass time of 8 seconds for alloy #6 and the results are shown in figure 7.18.

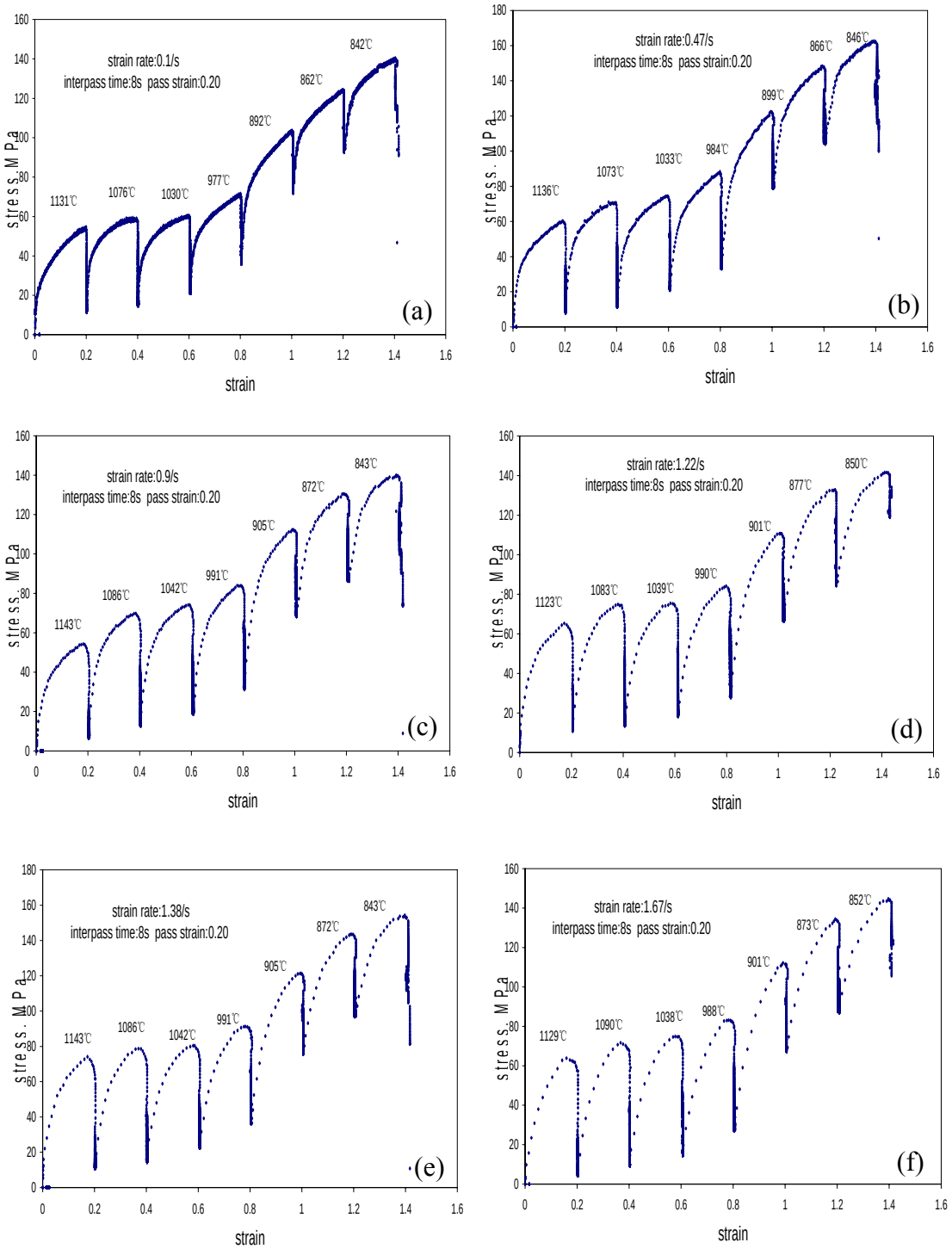

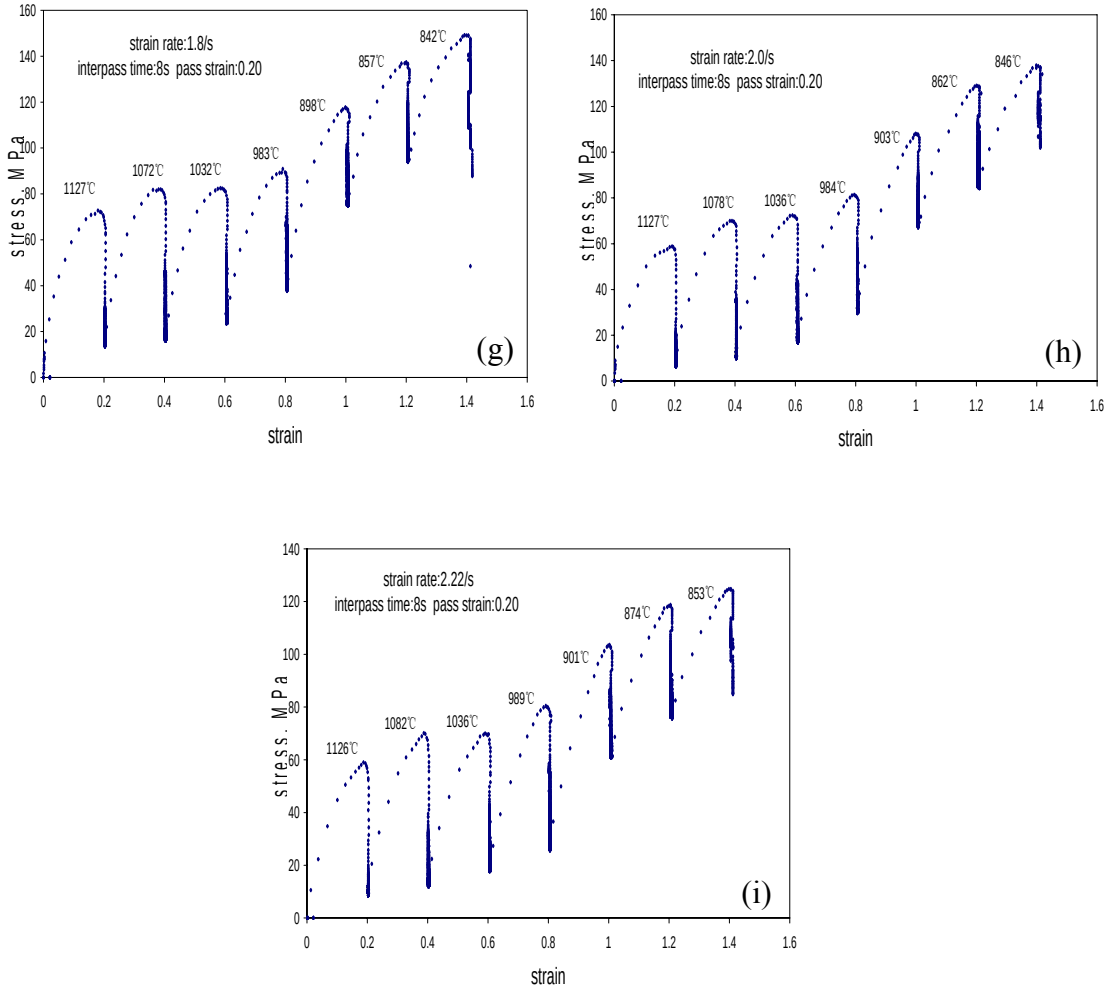

Figure 7.18 Stress-strain curves of compression deformation tests of alloy #6 at a constant pass strain of 0.20 and inter-pass time of 8 s but with a series of strain rates from 0.1 to 2.22 s^{-1}.

The number of passes in this series of tests was seven. The pass deformation temperatures are also marked on figure 7.18. The mean flow stresses calculated from figure 7.18 are plotted against the inverse of pass temperature (in K) in figure 7.19.

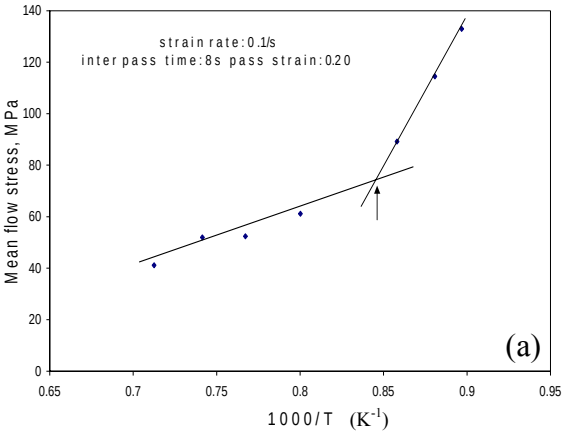

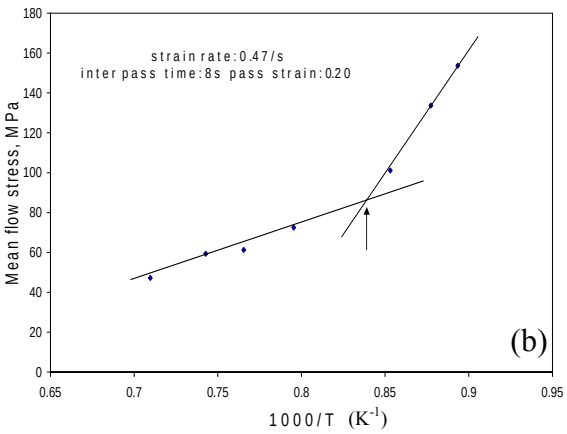

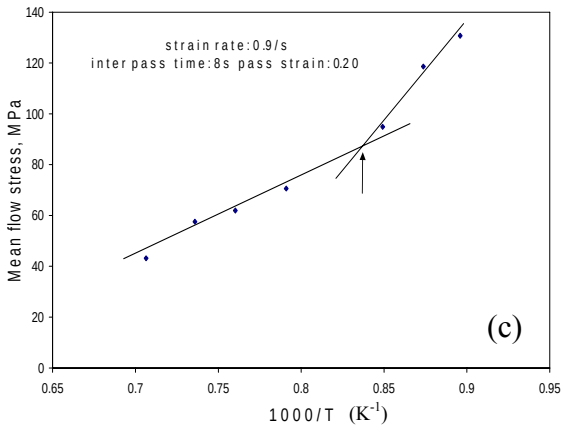

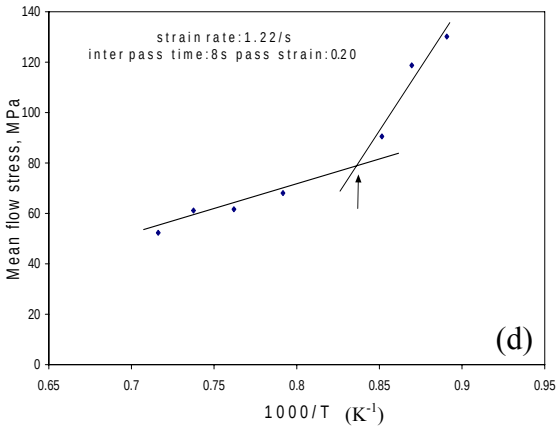

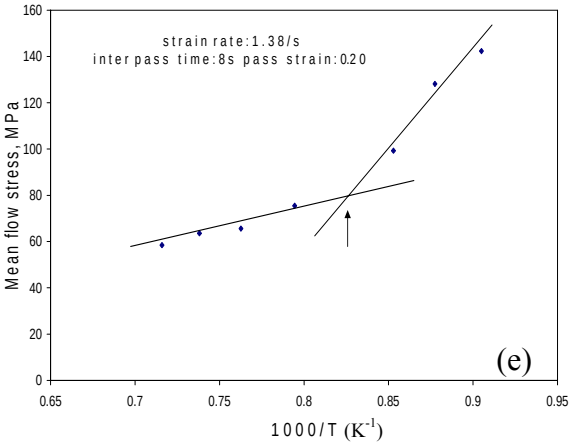

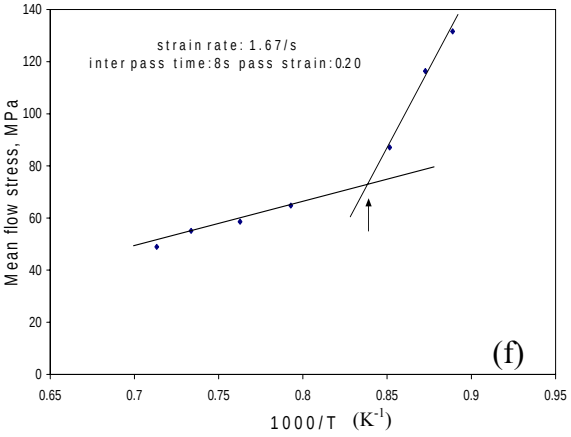

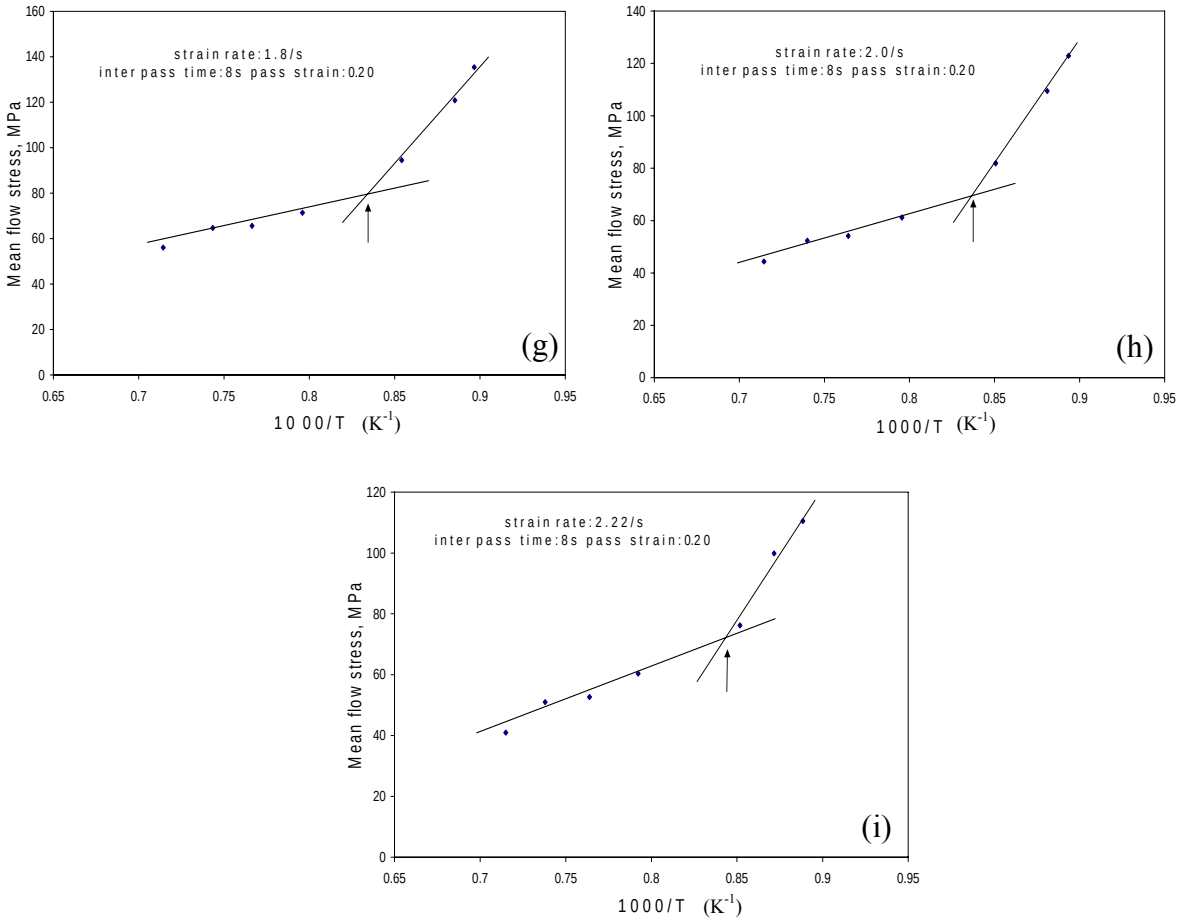

Figure 7.19 The mean flow stress versus inverse test temperature of alloy #6 at a constant pass strain of 0.20 and inter-pass time of 8 s but at a series of strain rates from 0.1 to 2.22 s^{-1}.

Table 7.6 The non-recrystallisation temperature and strain rates of alloy #6

Sample number	**C01**	**C05**	**C1**	**C15**	**C2**	**C3**	**C4**	**C6**	**C8**
Inter-pass time, t_{ip} (s)	8	8	8	8	8	8	8	8	8
Pass strain, ε	0.2	0.2	0.2	0.2	0.2	0.2	0.2	0.2	0.2
Strain rate (s^{-1})	0.1	0.47	0.9	1.22	1.38	1.67	1.80	2.0	2.22
T_{nr} (°C)	914	915	921	929	941	918	920	920	923

The results of the T_{nr} at different stain rates (with ε and t_{ip} constant) are listed in table 7.6 and are plotted in figure 7.20. The austenite should strain harden more at higher

strain rates during a compression test and this should result, theoretically at least, in a larger driving force for recrystallisation and, therefore, should decrease the T_{nr}. However, the opposite tendency was found in alloy #6 (see figure 7.20) and is also different from the results of Bai et al.[125] and Laasraoui[124]. They reported that the T_{nr} decreases with an increase in strain rate when the pass strains are 0.2, 0.3, 0.4 and 0.5. This inconsistency between these results and those obtained by others, may have to be examined further by torsion tests which allow higher strain rates than the highest value of 2.22 s^{-1} used here.

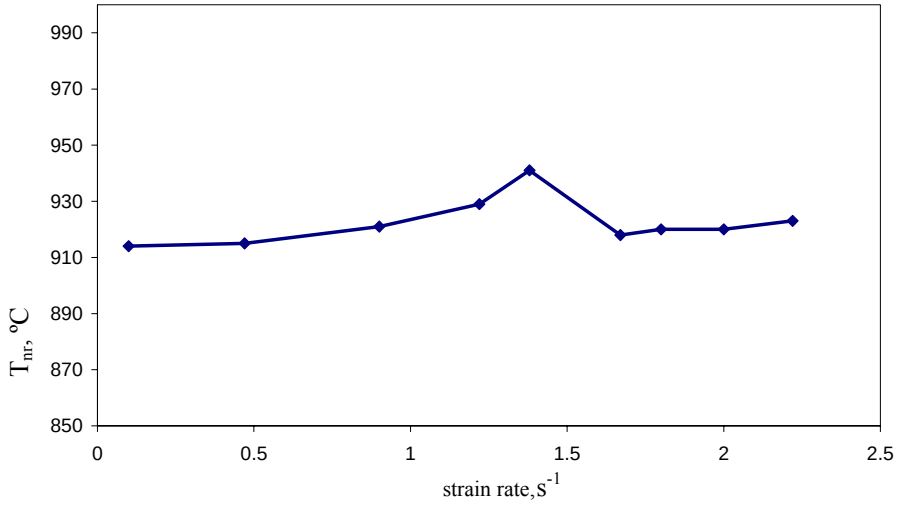

Fig.7.20 Strain rate ($\dot{\varepsilon}$) versus the non-recrystallisation temperature for alloy #6. Pass strain $\varepsilon = 0.2$, inter-pass time t_{ip}=8 s.